Built on
LDRD
Laboratory Directed Research
and Development

SAND20XX-XXXXR
LDRD PROJECT NUMBER: 211658
LDRD PROJECT TITLE: High-Resolution Raman Measurements of Gradients at Interfaces
PROJECT TEAM MEMBERS: Robert Barlow, Robert Harmon (8351)

ABSTRACT:

Fundamental investigations of non-equilibrium gas-liquid interfaces at elevated pressure will require knowledge of gas-phase boundary conditions affecting the interface structure. To assess the feasibility of applying one-dimensional imaging of spontaneous Raman scattering to resolve species and temperature gradients in the gas-phase boundary layer above a fluoroketone liquid surface, spectra of fluoroketone (1,1,1,2,2,4,5,5,5-nonafluoro-4-(trifluoromethyl)-3-pentanone) vapor in a carrier gas (N_2 or CO_2) are reported over the temperature range 300 K to 700 K. The measured Raman spectra show no detectable broadband interference from laser-induced fluorescence. Features of the fluoroketone Raman spectrum overlap the CO_2 spectrum, such that crosstalk corrections will be necessary for quantitative concentration measurements of CO_2 in mixtures. High-resolution Raman spectra in this overlap region, acquired over the same temperature range, will enable future development of temperature dependent spectral libraries for fluoroketone.

Spatially resolved profiles of Raman spectra (28 μm spacing) across the laminar gas-phase boundary layer above a fluoroketone liquid surface are demonstrated with the laser beam aligned vertically upward through the surface. Strong elastic scattering from the liquid is suppressed by a custom-designed spectrometer, which includes two long-pass filters with a combined optical density of 12. While the exact location of the gas-liquid interface cannot be identified from the present measurements, indications are that the gas-phase boundary layer can be resolved to within 30-60 μm of the liquid. These results provide a positive outlook for the application of 1D Raman scattering to measure quantitative species concentrations in gas-phase fluoroketone/CO_2/N_2 mixtures close to a liquid surface.

INTRODUCTION:

Gas-liquid interfaces are central to many natural and industrial processes, including evaporation [1], atmospheric-ocean gas exchange [2], Diesel fuel injection [3-5], carbon sequestration [6], enhanced oil recovery by gas injection [6] and formation of gas hydrates [7]. Fundamental understanding of gas-liquid interfaces is mainly limited to equilibrium conditions. However, heat and mass transfer across non-equilibrium interfaces is important in many systems, and fundamental questions remain about the chemical physics of transport across non-equilibrium multicomponent gas-liquid interfaces [8,9]. Such interfaces generally occur at elevated pressure and temperature in the presence of high temperature gradients, making them difficult to study experimentally.

Recent theoretical and experimental research on gas-liquid interfaces at elevated temperature and pressure have pointed to the existence of broadened, non-equilibrium interfaces,

Sandia National Laboratories is a multimission laboratory managed and operated by National Technology and Engineering Solutions of Sandia, LLC, a wholly owned subsidiary of Honeywell International, Inc., for the U.S. Department of Energy's National Nuclear Security Administration under contract DE-NA-0003525.

which are created at subcritical conditions in the presence of high temperature gradients. Dahms [10-15] developed a theoretical description of the transition of a multicomponent gas-liquid interface from a classical equilibrium two-phase interface to a broadened non-equilibrium interface. It has been postulated that this broadened interface between the vapor and liquid at subcritical temperatures and pressures results in unique transport properties in which the liquid diffuses into the surrounding gas, rather than evaporating [13]. In visualization experiments on high-pressure diesel fuel injection into combustion products at elevated temperature, Pickett and coworkers [16] observed qualitative changes in jet structure, suggesting a transition from subcritical spray breakup and droplet evaporation to dense fluid mixing with no visual indication spray ligaments or drops (Fig. 1). This was determined not to be a classical supercritical mixing problem because, while the pressure and temperature of the combustion products in the chamber were above the critical point of the liquid, the liquid was injected at subcritical temperature, and the interface itself formed at subcritical conditions.

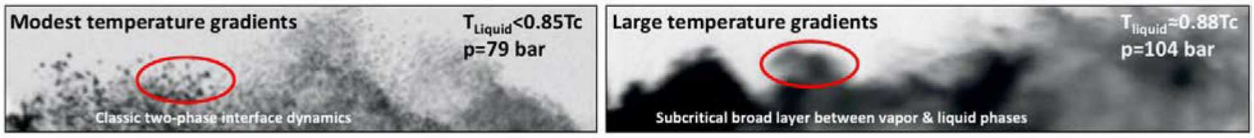

Fig. 1: Subcritical gas-liquid interface structure for injection of cold hydrocarbon fluid into different bath gas conditions. (Left) Classical two-phase dynamics with bath gas at 907 K and 79 bar. (Right) Diffuse mixing with large temperature gradients for bath gas at 1200 K and 104 bar. Consistent with theoretical predictions, region between vapor and liquid phases transforms from abrupt interface to a diffuse mixing layer that is observed for many microseconds, despite the conditions remaining subcritical. Images courtesy of L. M. Pickett, Sandia National Laboratories.

The present work was motivated by the need to develop novel quantitative diagnostic techniques for fundamental experimental investigation of gas-liquid interfaces undergoing the transition described above. Based on thermodynamic and physical properties, fluoroketone (1,1,1,2,2,4,5,5,5-nonafluoro-4-(trifluoromethyl)-3-pentanone with the structural formula $CF_3CF_2C(=O)CF(CF_3)_2$) was identified as a candidate liquid to be used in combination with CO_2 and N_2 in high-pressure multicomponent experiments. (This non-toxic, climate-friendly liquid is marketed by 3M^{TM} as a heat transfer fluid, Novec^{TM} 649 [17], and as a fire suppressant, Novec^{TM} 1230 [18].) Line imaging of spontaneous Raman scattering is a technique that could quantify the boundary conditions of interface as well as detect changes in the permeability of the interface. Ideally, concentrations of CO_2, N_2, and fluoroketone would be measured with sufficient spatial resolution and accuracy to fully characterize the species and temperature profiles across the gas-phase boundary layer adjacent to the interface, allowing conditions at the interface to be quantified by extrapolation. Raman spectra of N_2 and CO_2 may be calculated from theory over the relevant temperature range using the Ramses code from the Technical University of Darmstadt [19,20]. However, no published information on the Raman scattering spectrum of $C_6F_{12}O$ could be found to evaluate potential spectroscopic obstacles to such measurements, such as strong Raman crosstalk among the three species or excessive interference from laser-induced fluorescence of fluoroketone. Furthermore, no literature was found describing Raman scattering measurements of gas-phase boundary layers very close to liquid surfaces with the laser beam oriented normal to the surface.

The overall objective of the present work was to assess the feasibility of applying Raman scattering to investigate high-pressure gas-liquid interfaces in the fluoroketone/CO_2/N_2 system. Specific goals were: 1) to measure the Raman scattering spectrum of gas-phase fluoroketone over the temperature range (300 K–700 K) relevant to high pressure studies of the $C_6F_{12}O$/CO_2/N_2 system; and 2) to measure 1D Raman scattering profiles of these same species in a laminar boundary layer normal to a liquid fluoroketone surface, in order to assess the potential for highly-resolved measurements of scalar gradients near gas-liquid interfaces.

EXPERIMENTAL METHODS:

The major components of the experimental setup, shown in Fig. 2, include a 10W, 532-nm, TEM-00 laser (Lighthouse Photonics Sprout-G), a Raman spectrometer designed specifically for the present experiments, a liquid-nitrogen-cooled, low-noise, back-illuminated CCD camera (Princeton Instruments Versarray 1340 with 1300 × 1340 20-micron square pixels), a bubbler for evaporation of fluoroketone into a carrier gases, and a variac-controlled electrical heater for raising gas flow temperature.

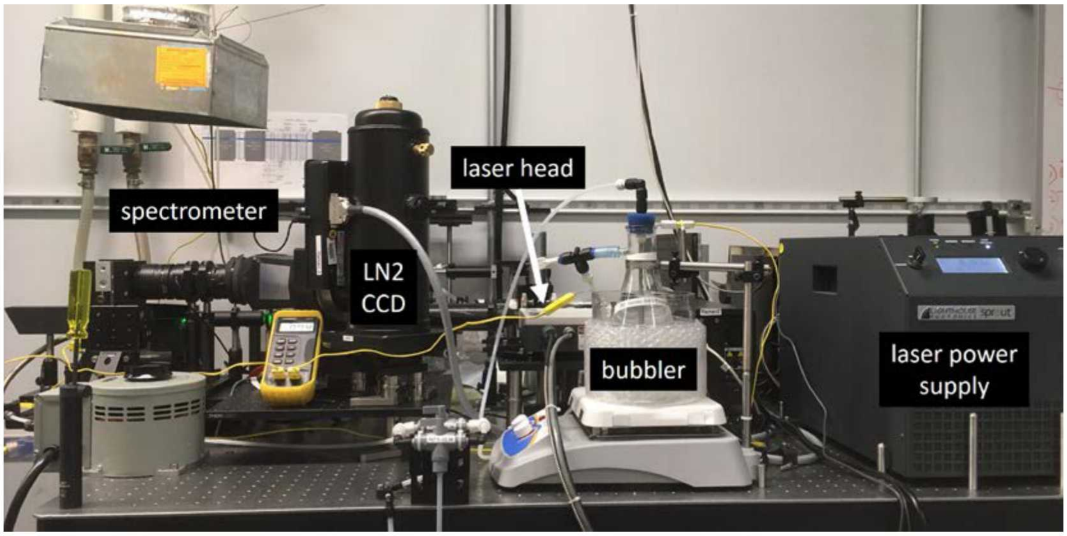

Fig. 2. Experimental setup for measuring gas-phase Raman scattering spectra over a range in temperature. The gas heater is mounted behind the spectrometer.

The spectrometer, illustrated in Fig. 3, consists of four 35-mm camera lenses (two Nikon 50-mm f/1.4, Nikon 85-mm f/1.4, and Canon 135-mm f/2), giving an overall design magnification of M = 1.59. Two long-pass optical filters (Semrock BLP01-532R-50.8-D), located in the collimated regions between the first and second pairs of lenses, block the laser wavelength with a combined optical density of roughly 12 at 532 nm. A 100-micron by 3-mm slit is located at the intermediate focal plane of the system to allow alignment of the imaged region very close to a surface without admitting excessive scattering from the liquid. A leaf shutter (Thorlabs SHB1T) is mounted in front of the slit for exposure control. The typical single-shot integration time was 0.5 s. Two custom high-transmission holographic gratings were used, as described below. The 2.3-mm diameter beam from the laser was expanded (Thorlabs GBE05-A, 5X beam expander) then focused by a 300-mm-fl AR coated lens to give an estimated Gaussian beam diameter of 18 microns.

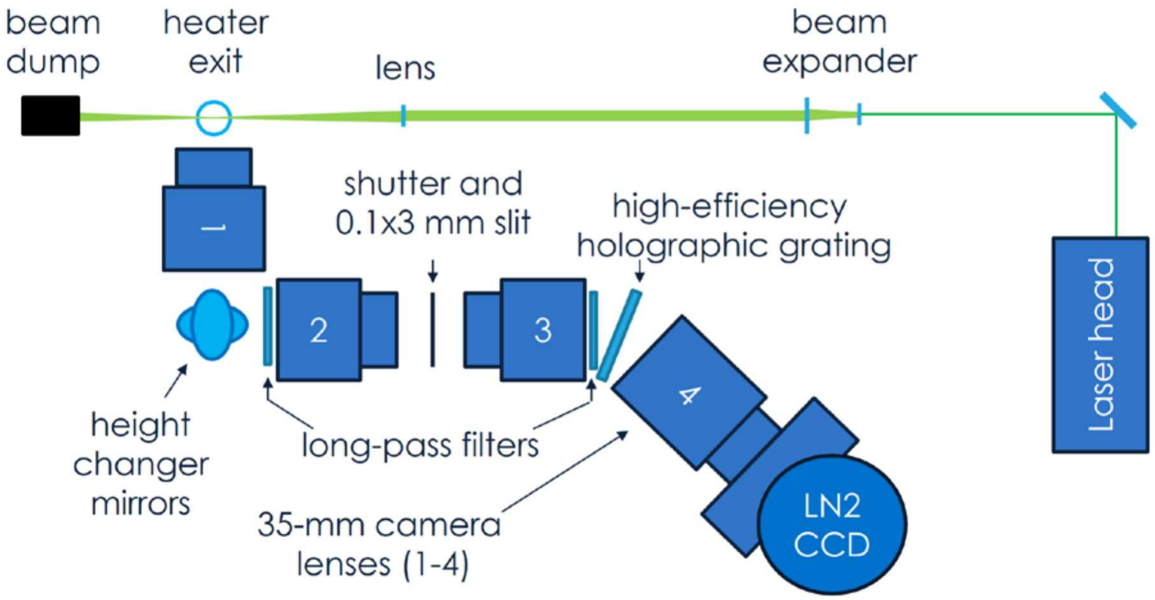

Fig. 3. Illustration (top view) of the spectrometer as configured for measurements of Raman scattering spectra of heated gases using the lower-dispersion grating.

Three different configurations of the spectrometer were used in three phases of the experiment. First, as illustrated in Fig. 3 and shown in Fig. 4a) the spectrometer was assembled with a height changer between the first two lenses to rotate the image of the horizontal laser beam that was focused above the exit of the gas heater. A grating with relatively low dispersion (Kaiser Optical VPH-1200-625, 1200 line/mm, 625 nm center wavelength, 44º turning angle) was used to allow simultaneous measurement of the Raman spectra of all three species of interest. Second, (Fig. 4b) a high-dispersion grating (Kaiser Optical HDG-573, 573 nm center wavelength, 4165 lines/mm, double-pass, 90º turning angle) was substituted to allow higher resolution measurements of the $C_6F_{12}O$ Raman spectrum in the region of overlap with CO_2. Third, (not shown) for measurements of the gas-phase boundary layer above a fluoroketone surface, using a vertical alignment of the laser beam, the height changer was removed and the lower resolution grating was reinstalled.

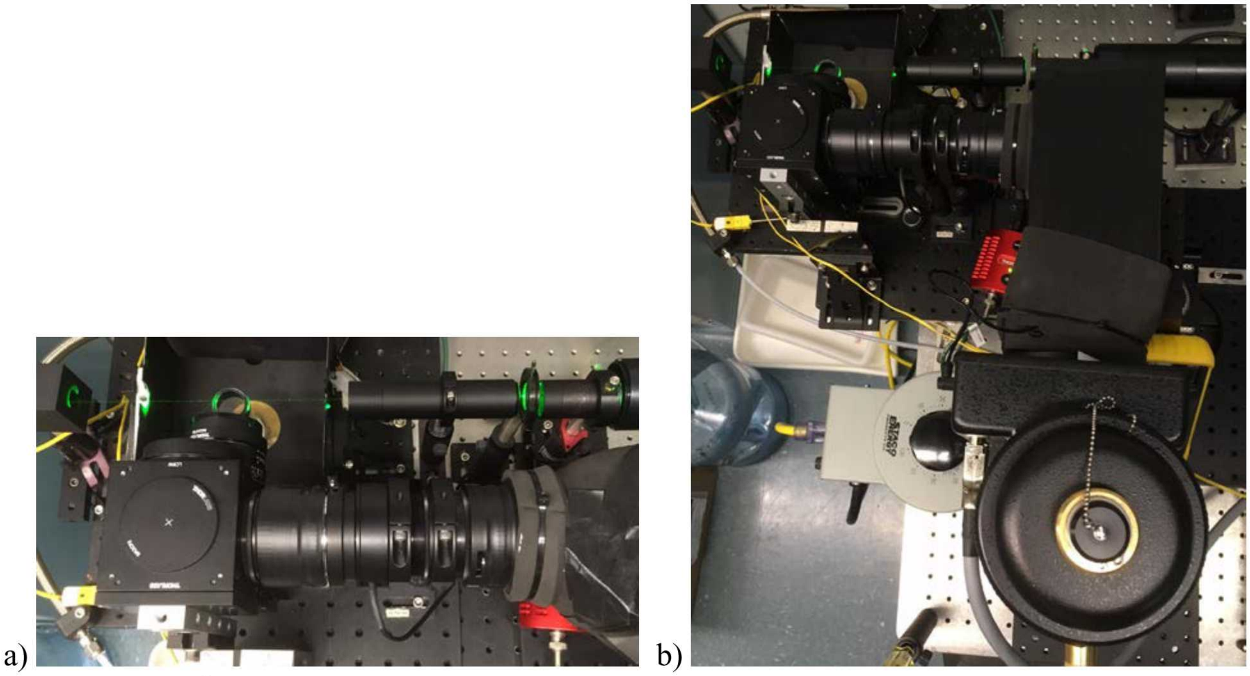

Fig. 4. a) Top view of the spectrometer configuration for heated gas measurements at low-dispersion, as in Fig. 2, showing the laser focus above the heater exit and the optical components in front of the grating. b) Spectrometer and camera configuration for the high-dispersion measurements.

The overall magnification of the optical system was measured by using a neon lamp to back-illuminate a precision laser-drilled metal foil target aligned at the object plane of the spectrometer, yielding a projected pixel resolution of 14.06 microns. This target had a linear pattern of 50-micron diameter holes spaced by 200 microns. Spectral calibration was accomplished using the same neon-illuminated target. The range of this spectral calibration was extended toward the blue by measuring the Raman scattering spectrum from a room temperature mixture of nitrogen and hydrogen and adding the theoretically calculated wavelength values for the N_2 peak and H_2 S-branch rotational lines to the known neon atomic lines. These spectra, acquired with the lower resolution grating, are combined in Fig. 5, and the resulting pixel to wavelength calibration was implemented as:

$$\lambda(\mathrm{nm}) = -\,2.081\mathrm{e}\text{-}09 * n^3 + 1.729\mathrm{e}\text{-}06 * n^2 + 0.1174 * n + 535.2,$$

where n is the CCD pixel number. This calibration requires alignment of the laser beam to place the N_2 peak on pixel 613, which corresponds to the center of the 100-micron slit image. This alignment was accomplished with the vertical adjustment on the mount for the final focusing lens. Spectral calibration of the high dispersion setup was accomplished by fitting the peaks in the measured spectrum of a mixture of H_2 and CO_2 at 294 K:

$$\lambda(\mathrm{nm}) = -\,8.7741\mathrm{e}\text{-}07 * n^2 + 1.7887\mathrm{e}\text{-}02 * \mathrm{n} + 555.69.$$

The high dispersion grating gives better spectral resolution by a factor of 6.9 in the region of overlap of fluoroketone and CO_2 spectra (0.0168 nm/pixel), which will facilitate the construction of temperature dependent spectral libraries for fluoroketone to be used in correcting for crosstalk in future application to multicomponent measurements at elevated pressure.

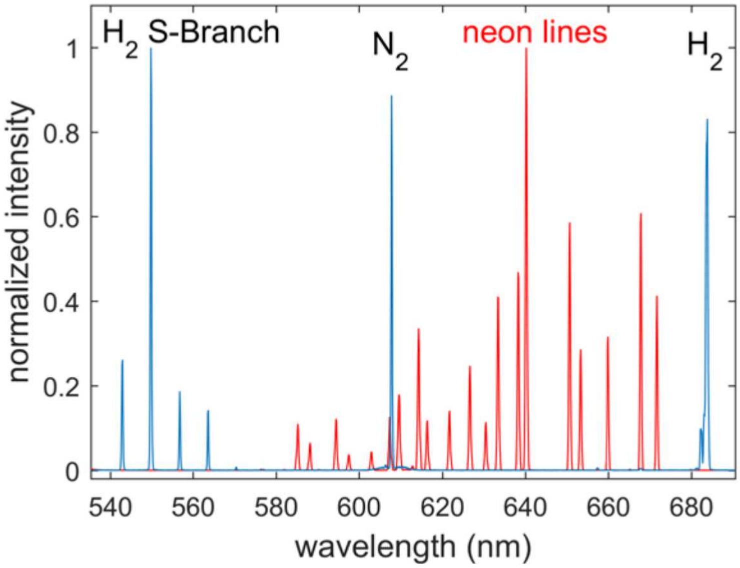

Fig. 5. Combined spectra of neon atomic lines from back-illumination of a 50-micron pinhole and Raman scattering spectra from a 295 K mixture of N_2 and H_2. Six S-branch rotational lines of H_2 are detectable (two at very low signal levels) in the region 540 nm < λ < 580 nm.

Fluoroketone has a high vapor pressure of 40.4 kPa at 25ºC [19], allowing for convenient evaporation into a carrier gas passed through a bubbler. N_2 or CO_2 was passed through the bubbler to deliver fluoroketone to the heater. The bubbler was placed in a water bath on a temperature-controlled, stirring hot plate, and temperatures of the fluoroketone liquid and the heated gas were monitored using type K thermocouples. Due to the high evaporation rate of the liquid, a valve system was built to allow rapid manual switching of the carrier gas to flow through bubbler or directly to the heater in combination with an additional gas stream. This strategy minimized use of the fluoroketone and also minimized evaporative cooling of the liquid reservoir. The reservoir was refilled to a marked level before each measurement to help ensure repeatability of the evaporation process.

The heater, shown schematically in Fig. 6, has a silicon carbide element within a quartz tube and gas inlet ports below the heater. A 0.25-mm diameter shielded type K thermocouple was positioned roughly 1 cm below the exit and aligned beneath the laser probe volume to measure the temperature of the gas.

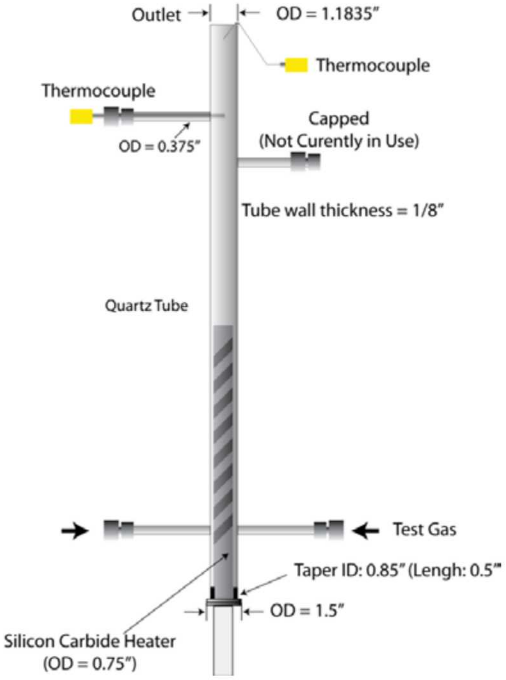

Fig. 6. Electric heater and thermocouple configuration. Three inch fiberglass insulation around the quartz tube is not shown.

For each target temperature, Raman spectra were acquired with and without fluoroketone (bubbler bypassed). Due to the high heat capacity of fluoroketone, the total gas flow for measurements that bypassed the bubbler had to be increased in order to achieve the same heater exit temperature. Appropriate flow rates were identified at the highest target temperature (700 K), and the temperatures were subsequently reduced in 25 K or 50 K steps. Marching down in temperature allows the thermal capacitance of the heater assembly to contribute to the heating of the gas flow, such that target exit temperatures are achieved with lower current to the silicon carbide heating element. This strategy reduces the potential for thermal decomposition of fluoroketone in contact with a heater element at temperatures significantly higher than the target temperature. (Note: $3M^{TM}$ product literature indicates thermal stability to greater the 300 C in the absence of contact with water. However, the MSDS lists “no data available” for decomposition temperature. Initial measurements ramping up in temperature showed some inconsistency in shapes of spectral feature.)

The flow facility illustrated in Fig. 7 was built for measurements of the gas-phase boundary layer above a liquid fluoroketone surface. Commercially available glass cells did not have the desired geometric features, so a cell was constructed from microscope slides and 5-minute epoxy. The long length (600 mm) of aluminum tubing ahead of the cell ensures laminar flow. An open syringe and dispensing needle, crimped at the end to limit flow, served as a reservoir (“IV drip”) to compensate for the rapid evaporation of fluoroketone and maintain constant fluid level in the cell during data acquisition. Liquid and gas temperatures were measured using 0.25-mm diameter shielded type-K thermocouples. A rectangular mask with a height of 8 mm was placed in front of the collection lens, with the lower edge of the open area aligned with the fluid surface level and optical axis. This prevented collection of light rays passing downward through the liquid, and it also served to reduce the blurring effect of the cell wall in the vertical direction.

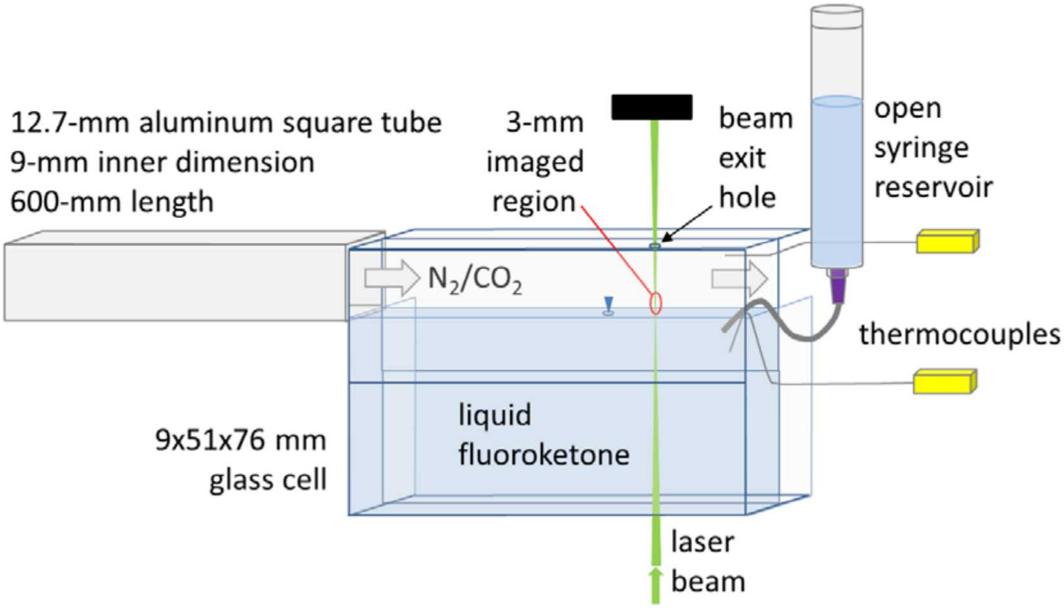

Fig. 7. Setup for laminar boundary layer measurements over a liquid surface.

RESULTS:

As discussed above, no literature on the spectroscopy of this or similar fluoroketones was found to allow assessment of potential fluorescence interference or Raman crosstalk in Raman scattering measurements of the multicomponent gas-phase system of interest ($C_6F_{12}O$, CO_2, and N_2). Figure 8 shows that there is no detectable broadband fluorescence in measured room temperature Raman scattering spectrum from a mixture of fluoroketone and N_2. All measurements at elevated temperature also had flat baselines, so fluorescence interference can be eliminated as a potential problem for quantitative application of Raman scattering in systems with this fluoroketone. Note also that there is no indication of leakage of the 532-nm laser light onto the detector for these gas-phase measurements.

The fluoroketone spectrum shows several features within the range $535 < \lambda < 590$ nm (transition energies between 100 cm^{-1} and 1800 cm^{-1}). However, assignment of vibrational modes is beyond the scope of the present work, and we will focus on temperature dependence of the spectrum, particularly in the region of overlap with CO_2. This overlap is highlighted in Fig. 9, which shows separately measured spectra of fluoroketone and CO_2. It is clear that multicomponent measurements will require correction for crosstalk of fluoroketone onto CO_2. Strategies for such a correction will be discussed in the next section.

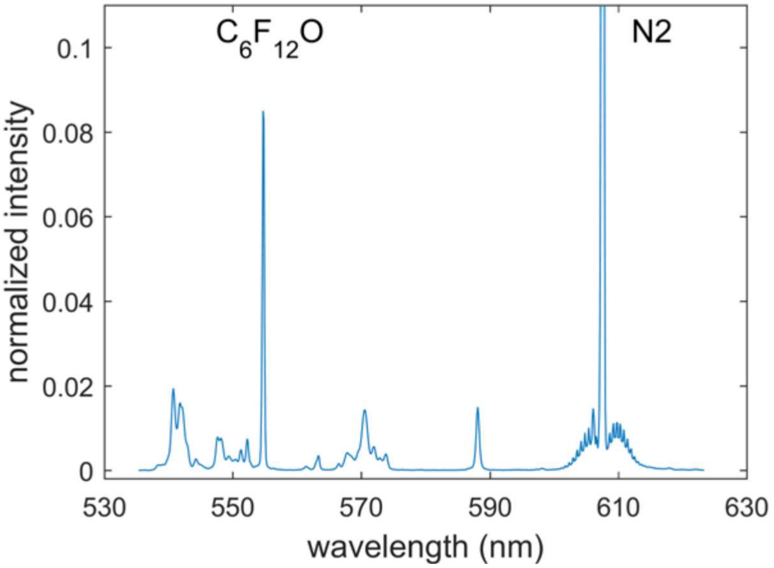

Fig. 8. Measured Raman scattering spectrum from a mixture of six percent $C_6F_{12}O$ in N_2 at 297 K normalized by the peak N_2 intensity.

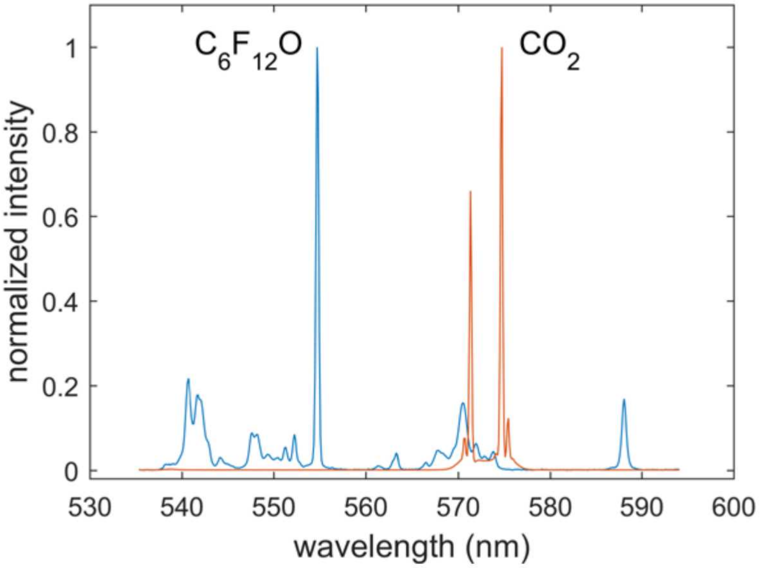

Fig. 9. Separately measured spectra of $C_6F_{12}O$ and CO_2 at 297 K, showing overlap in the region from 568 nm to 575 nm (1180—1340 cm^{-1}).

Figures 10a and 10b show fluoroketone spectra acquired in $N_2/C_6F_{12}O$ mixtures in two sequences at temperature intervals of roughly 50 K between room temperature and 700 K. Twenty exposures of 0.5 s were acquired and averaged for each measurement condition. The temperature series was run twice, starting from the highest temperature, to provide insight repeatability. Here the intensity in each spectrum has been scaled by the temperature ratio *T*/297 K to remove the density effect and then normalized by the peak value in the lowest temperature spectrum in the series. The gradual transition in the shape of each spectral feature suggests that thermal decomposition is not an issue within the measured temperature range, when using the strategy of starting at the highest temperature. In contrast, initial measurements ramping up in temperature showed some inconsistencies in spectral features near 540 nm suggesting the possibility of thermal decomposition of fluoroketone in contact with the heating element at a temperature significantly higher than the target temperature.

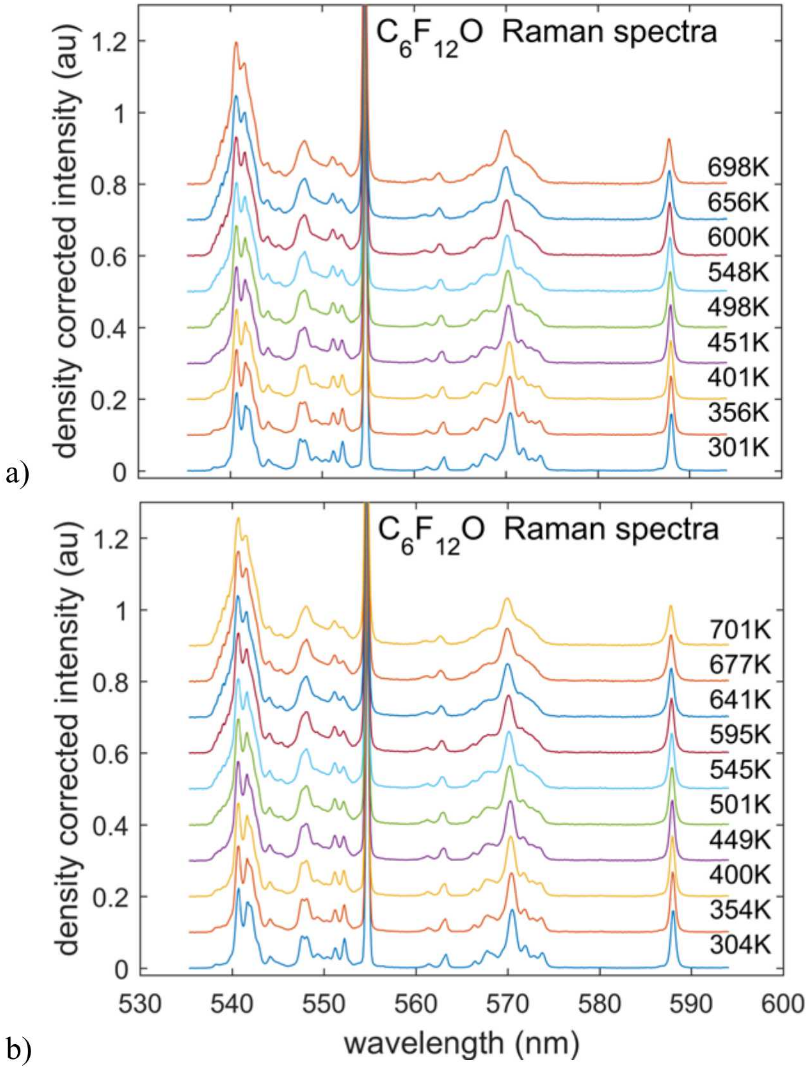

Fig. 10. Normalized fluoroketone spectra at the indicated temperatures from two series of measurements, each starting at roughly 700 K and progressing to lower temperatures.

The mole fraction of fluoroketone must be determined from the Raman measurement of the N_2 carrier gas at each temperature. A calibration measurement of pure N_2 at room temperature combined with the theoretically derived temperature dependence of the integrated N_2 Raman scattering intensity allowed the expected signal from pure N_2 to be calculated for each elevated temperature condition. The mole fractions of N_2 and fluoroketone were then calculated from the measured N_2 signal, yielding an average value of 0.099 with a standard deviation of 0.005 for the fluoroketone mole fraction, compared to roughly 0.12 for saturated vapor.

A likely strategy for quantitative measurements of fluoroketone concentration in gas mixtures will be to integrate the signal within the interval $535 < \lambda < 560$ nm by binning on-chip for each spatially resolved increment. This approach suppresses the effect of camera readout noise. Figure 11 shows the integrated response of fluoroketone over this spectral region, corrected for density and mole fraction at the local temperature and normalized by the integrated response of N_2 at 294 K. The effective Raman cross section increases linearly with temperature from 7.2 times N_2 at room temperature to roughly 13 times N_2 at 700 K, grating efficiency effects excluded. Repeatability of the measured relative response for the two series is quite satisfactory.

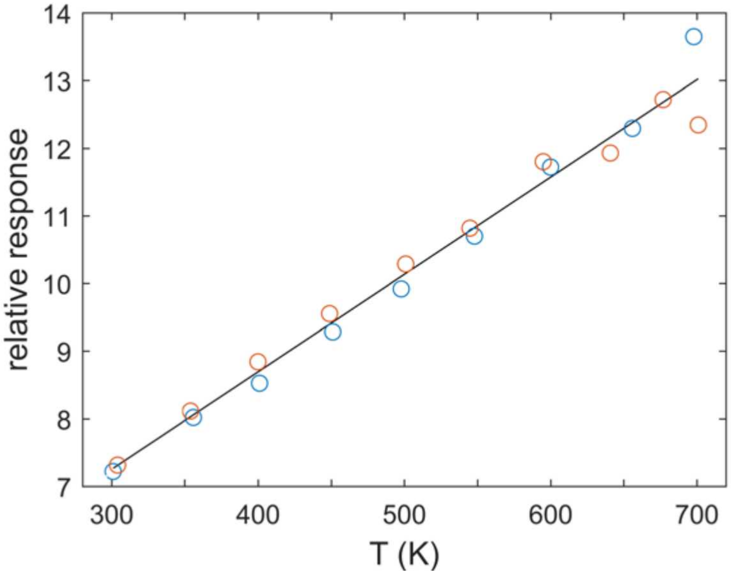

Fig. 11. Response of fluoroketone for the two temperature series (different symbol colors), integrated over the spectral interval $535 < \lambda < 560$ nm, corrected for density and mole fraction, and normalized by the integrated N_2 response at 294 K.

As shown in Fig. 9, there is overlap of the CO_2 and fluoroketone spectra. This region of overlap was investigated in more detail using the high-dispersion grating. Measured Raman scattering spectra of CO_2, CO_2 plus fluoroketone (CO_2 passing through the bubbler), and fluoroketone without CO_2 (N_2 passing through the bubbler) are shown in Fig. 12. The fact that the spectral features of fluoroketone are significantly broader than those of CO_2 has implications for correction procedures that will need to be developed for quantitative concentration measurements in fluoroketone/CO_2/N_2 mixtures. This will be discussed in the next section.

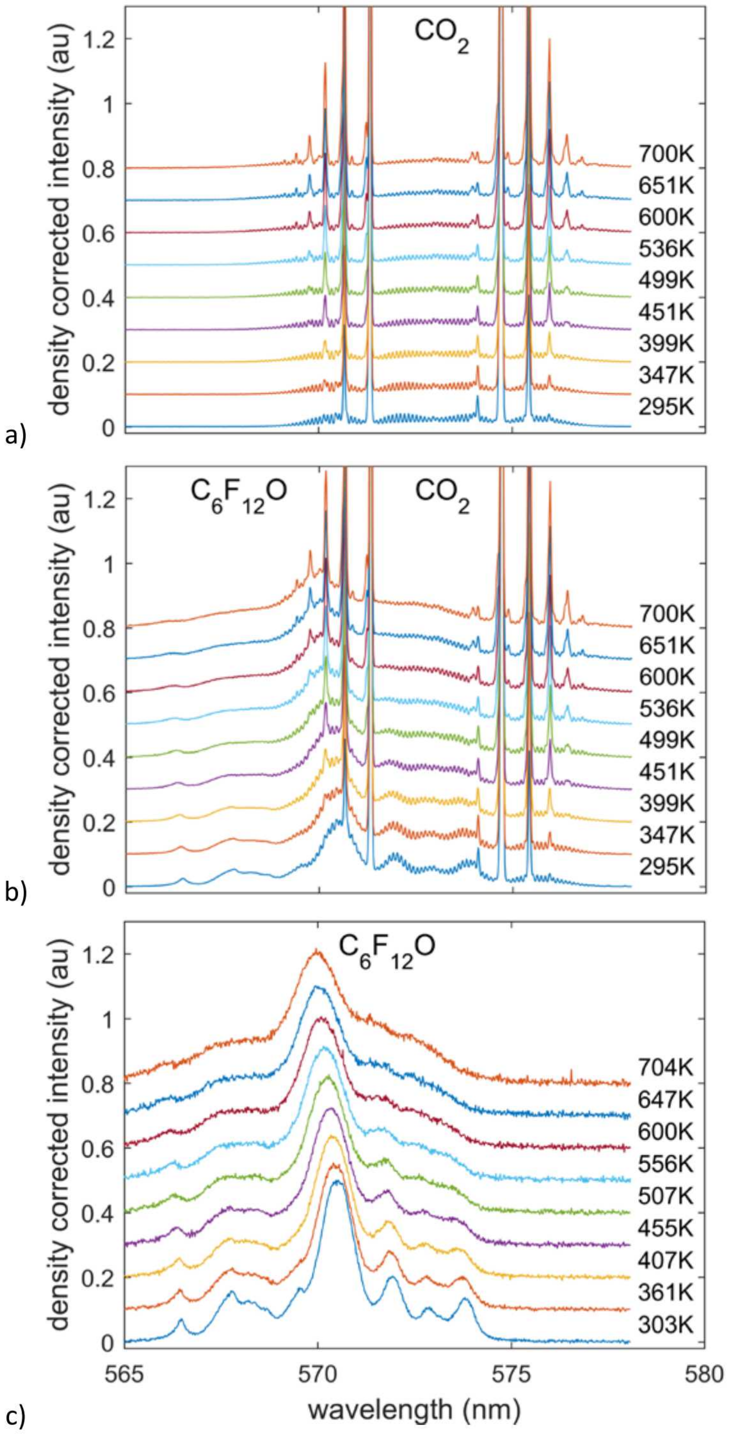

Fig. 12. Density corrected spectra of a) CO_2; b) CO_2 plus $C_6F_{12}O$; and c) $C_6F_{12}O$ without CO_2. Each spectrum in a) and b) is normalized by the maximum in the lowest temperature spectrum, while twice the maximum is used in c).

The second major objective of this work was to measure 1D Raman scattering profiles of fluoroketone, CO_2, and N_2 in a laminar boundary layer above a liquid fluoroketone surface, in order to assess the potential for highly-resolved measurements of scalar gradients near gas-liquid interfaces. For these measurements, the lower half of the collection lens was masked, and liquid surface was position on the optical axis of the lens. Laser power was reduced to 4 W to avoid burning the bottom of the cell or boiling fluoroketone at the location of beam penetration. Camera pixels were binned by 2 in the spatial dimension for a projected pixel spacing of 28.12 μm. A 2:1 ratio of CO_2 to N_2 was used to more easily identify the CO_2 spectral features in the region of overlap with $C_6F_{12}O$. With steady laminar flow and a constant fluid level, images could be averaged over multiple exposures to reduce noise. Figure 13 shows vertical profiles of the integrated intensity of the fluoroketone signal within the interval $535 < \lambda < 560$ nm averaged over the first and last halves of a 50-image sequence, each with 0.5 s exposure. Here, the intensities have been normalized by the expected intensity for saturate fluoroketone vapor in equilibrium with the liquid surface (dashed red line in the figure). As expected, the measured profiles show a large change in the gradient of the Raman scattering intensity of fluoroketone near the interface. The precise surface location is not known, and the zero position is assigned approximately. There is a shift of only 0.015 mm (roughly half the binned pixel spacing) between the average profiles from the two halves of the data set, as indicated by the dashed black line in Fig. 13, confirming good control of the surface level.

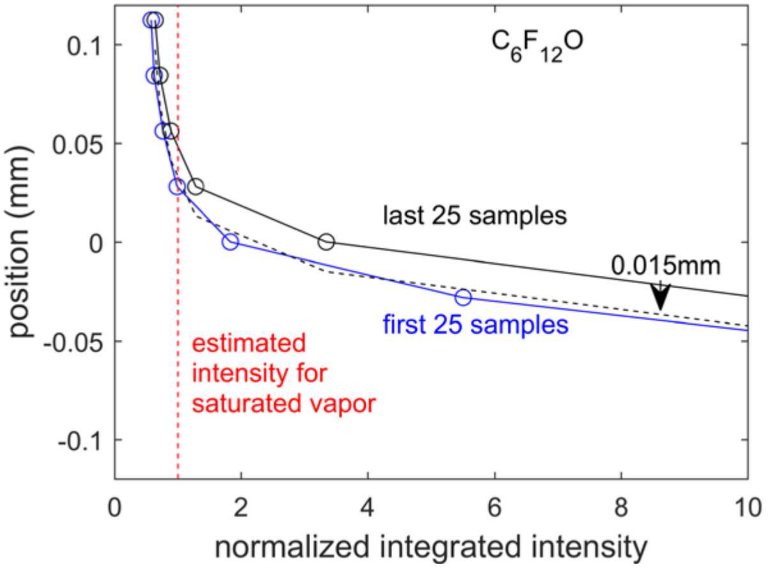

Fig. 13. Spatial profiles of the integrated intensity of fluoroketone over the interval $535 < \lambda < 560$ nm near the gas-liquid interface. Profiles are normalized by the estimated intensity for saturated vapor in equilibrium with the liquid. The data spacing is 0.028 mm. The dashed black line represents the average profile for the last 25 samples, shifted downward by 0.015 mm.

Raman spectra (50-image averages), are plotted in Fig. 14 for six evenly spaced locations across the laminar gas-phase boundary layer. Based on vapor pressure data from 3M^{TM}, the equilibrium mole fraction of fluoroketone vapor at the gas-liquid interface should be close to 0.4, and the mole fractions of CO_2 and N_2 should be close to 0.4 and 0.2, respectively. Quantitative conversion of the measured spectra to species concentrations at each location would require development of temperature dependent spectral libraries for fluoroketone and analysis by spectral fitting, which are beyond the scope of the present exploratory investigation. It is qualitatively apparent that the fluoroketone signal decreases with increasing distance from the interface, while the CO_2 and N_2 signals increase. However, the imaged region does not extend all the way to the free stream, where the mole fractions of CO_2 and N_2 would be 0.67 and 0.33 respectively. At the measurement location, 50 mm from the leading edge of the gas-liquid interface, the scalar boundary layer thickness already exceeds the length of the Raman scattering probe volume.

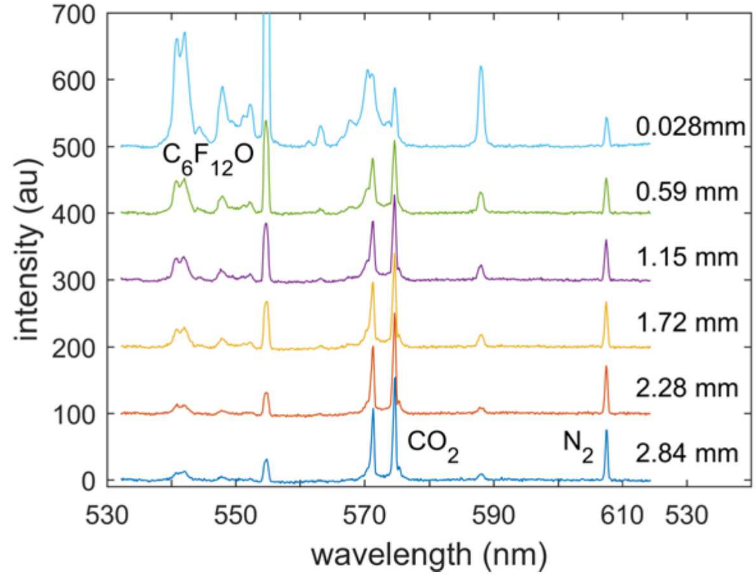

Fig. 14. Averaged Raman spectra from six evenly spaced locations across the gas-phase boundary layer above the fluoroketone liquid surface.

DISCUSSION:

Results show that this fluoroketone (Novec^{TM} 649) is actually friendly to Raman scattering diagnostics in the context of multicomponent gas-phase measurements with CO_2 and N_2. The large relative scattering cross section, absence of detectable laser-induced fluorescence under 532 nm excitation, and negligible crosstalk onto N_2 in gas-phase mixtures all point to excellent prospects for quantitative concentration measurements over the relevant temperature range (300 K to 700 K).

The next steps toward development of quantitative methods will be: 1) to construct temperature dependent spectral libraries for fluoroketone; and 2) to develop data analysis approaches to correct for crosstalk of fluoroketone onto CO_2. In previous work [21,22], spectral libraries for several small hydrocarbons were developed by representing measured Raman spectra as a family of Gaussians and fitting the evolution of their parameters as functions of temperature. This only needs to be done for fluoroketone in the region of overlap with CO_2. Quantifying the fluoroketone concentration in mixtures with CO_2 and N_2 can be accomplished by integrating the spectral intensity within the interval $535 < \lambda < 560$ nm (by binning on-chip or in software) for each spatially resolved increment.

The integrated fluoroketone response relative to N_2, shown above in Fig. 11, does not account to the wavelength dependence of grating efficiency, so additional work would be needed to accurately determine the absolute Raman scattering cross section. Furthermore, because there is some uncertainty in the fluoroketone mole fraction, as determined in the present experiments, it would be beneficial to measure Raman spectra of pure fluoroketone and pure N_2 in a cell, just at room temperature. Alternatively, the bubbler design could be improved to ensure full saturation at a tightly controlled temperature.

With respect to corrections for crosstalk of fluoroketone onto CO_2, the fact that spectral features of CO_2 are much narrower than those of fluoroketone, at least with the present spectrometer and small laser beam diameter, suggests that a spectral fitting approach may be preferable to the hybrid matrix inversion method [23], which was developed for analysis of single-shot Raman measurements in turbulent flames. A spectral fitting approach could be particularly beneficial for measurements close to the liquid surface, where the integrated fluoroketone signal in the overlap region can significantly exceed that of CO_2 (see Fig. 14).

ANTICIPATED OUTCOMES AND IMPACTS:

A proposal for a new program of fundamental investigation of the physics of high-pressure, non-equilibrium, gas-liquid interfaces was recently submitted to DOE/BES and is under review. This proposal was submitted before any of the present experiments were completed, so potential obstacles to the application of Raman scattering in this context had to be acknowledged. The success of the present exploratory experiments provides clear evidence to support the proposed high-pressure Raman scattering experiments, as well as the choice of fluoroketone/CO_2/N_2 as the target system. Fluoroketone has relatively low critical temperature and pressure (442 K, 18.7 bar). Alternative liquids with higher critical conditions would increase the cost and complexity of experiments. If reviewers are skeptical of the approach or its chances for success, the present results would contribute to a compelling rebuttal. If the proposal is funded, then the present results will give us a significant head start on diagnostic development, as well as confidence to design the high-pressure facility with specifications appropriate for the fluoroketone/CO_2/N_2 system.

In brief, the DOE proposal outlines 1D Raman scattering measurements of temperature and species concentrations in the gas-phase boundary layer above a liquid fluoroketone surface in a high-pressure apparatus, conceptually illustrated in Fig. 15 (right side). A laminar flow of heated CO_2/N_2 gas would impinge on the surface. A suite laser diagnostics with potential for sensitivity to the interface thickness was proposed in combination with Raman scattering diagnostics for the gas-phase. These Raman measurements will serve to quantify the boundary conditions for the interface and determine where in the parameter space of pressure, temperature, and temperature/concentration gradients the transition occurs from a classical equilibrium two-phase interface to a broadened, non-equilibrium, dense-fluid interface. According to theory, this transition should significantly increase the permeability of the interface, altering the relationship between temperature and species mole fractions across the whole of the boundary layer. Thus, the Raman measurements have potential to yield the first quantitative experimental confirmation of the Sandia-developed theory describing these broadened interfaces.

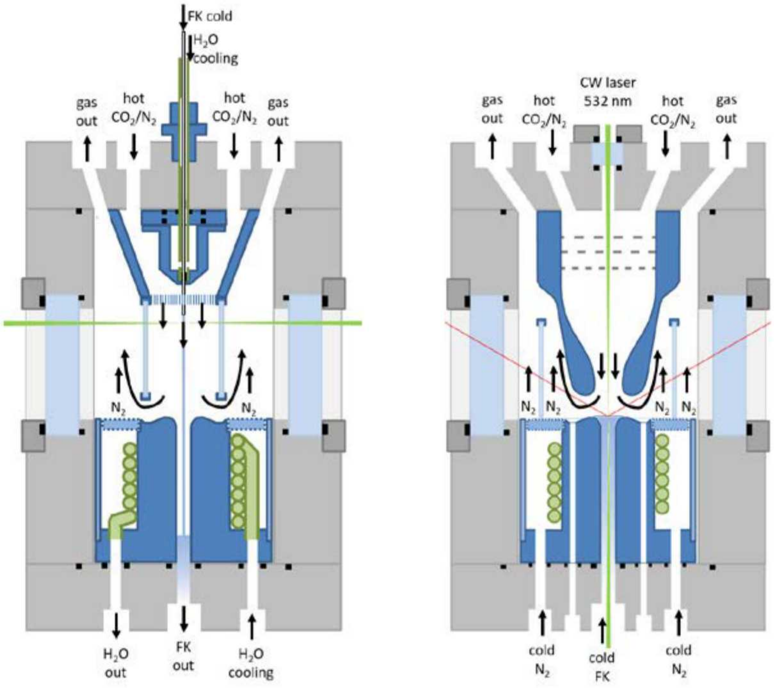

Fig. 15. Conceptual designs for high-pressure investigations of gas-liquid interfaces in laminar jet (left) and laminar counterflow (right) configurations.

Demonstration of spatially-resolved, surface-normal measurements of a laminar gas-phase boundary layer by 1D Raman scattering has relevance to research on gas-solid interfaces as well as gas-liquid interfaces. As a quick demonstration test, a 400 μm hole was drilled through a thin aluminum plate, which was aligned in place of the liquid surface, such that the laser beam passed through the hole, and 1D images of Raman scattering from ambient air were recorded. A proposal to investigate coupled gas-phase and surface kinetics was recently approved by DOE/BES, and, while not included in the current statement of work, there is potential to apply 1D Raman scattering to measure most of the major species in the gas-phase boundary layer above a catalytic surface in atmospheric (or higher) pressure oxidative methane coupling.

CONCLUSIONS:

Fundamental investigations of non-equilibrium gas-liquid interfaces at elevated pressure will require knowledge of gas-phase boundary conditions affecting the interface structure. To assess the feasibility of applying one-dimensional imaging of spontaneous Raman scattering to resolve species and temperature gradients in the gas-phase boundary layer above a fluoroketone liquid surface, Raman scattering spectra of fluoroketone (1,1,1,2,2,4,5,5,5-nonafluoro-4-(trifluoromethyl)-3-pentanone) vapor in a carrier gas (N_2 or CO_2) were measured over the temperature range 300 K to 700 K. The measured Raman spectra show no detectable broadband interference from laser-induced fluorescence. Features of the fluoroketone Raman spectrum overlap the CO_2 spectrum, such that crosstalk corrections will be necessary for quantitative concentration measurements of CO_2 in mixtures. High-resolution Raman spectra in this overlap region, acquired over the same temperature range, will enable future development of temperature dependent spectral libraries for fluoroketone, which will be required for such corrections.

Spatially resolved profiles (with 28 μm spacing) of Raman spectra across the laminar gas-phase boundary layer above a fluoroketone liquid surface were demonstrated with the laser beam aligned vertically upward through the surface. Strong elastic scattering from the liquid was effectively suppressed by a custom-designed spectrometer, which included two long-pass filters with a combined optical density of 12. While the exact location of the gas-liquid interface could be identified from the present measurements, indications are that the gas-phase boundary layer can be resolved to within 30-60 μm of the liquid. These results provide a positive outlook for the application of 1D Raman scattering to measure quantitative species concentrations in gas-phase fluoroketone/CO_2/N_2 mixtures close to a liquid surface.

REFERENCES:

[1] S.I. Anisimov, D.O. Dunikov, V.V. Zhakhovskii, S.P. Malyshenko, Properties of a liquid–gas interface at high-rate evaporation, J. Chem. Phys. 110 (1999) 8722-8729.

[2] L.F. Phillips, Processes at the gas-liquid interface, Int. Rev. Phys. Chem. 30 (2011) 301-333.

[3] X. Jiang, G.A. Siamas, K. Jagus, T.G. Karayiannis, Physical modelling and advanced simulations of gas-liquid two-phase jet flows in atomization and sprays, Prog. Energy Combust. Sci. 36 (2010) 131-167.

[4] A.L.N. Moreira, A.S. Moita, M.R. Panao, Advances and challenges in explaining fuel spray impingement: How much of single droplet impact research is useful?, Prog. Energy Combust. Sci. 36 (2010) 554-580.

[5] M.P.B. Musculus, P.C. Miles, L.M. Pickett, Conceptual models for partially premixed low-temperature diesel combustion, Prog. Energy Combust. Sci. 39 (2013) 246-283.

[6] K.B. Haugen, A. Firoozabadi, Composition at the interface between multicomponent nonequilibrium fluid phases, J. Chem. Phys. 130 (2009) 064707.

[7] X. Fu, L. Cueto-Felgueroso, R. Juanes, Nonequilibrium thermodynamics of hydrate growth on a gas-liquid interface, Phys. Rev. Lett. 120 (2018) 144501.

[8] G. Castiglioni, J. Bellan, On models for predicting thermodynamic regimes in high-pressure turbulent mixing and combustion of multispecies mixtures, J. Fluid Mech. 843 (2018) 536-574.

[9] E. Masi, J. Bellan, K.G. Harstad, N.A. Okong'o, Multi-species turbulent mixing under supercritical-pressure conditions: modelling, direct numerical simulation and analysis revealing species spinodal decomposition, J. Fluid Mech. 721 (2013) 578-626.

[10] R.N. Dahms, Gradient Theory simulations of pure fluid interfaces using a generalized expression for influence parameters and a Helmholtz energy equation of state for fundamentally consistent two-phase calculations, J. Colloid Interface Sci. 445 (2015) 48-59.

[11] R.N. Dahms, Understanding the breakdown of classic two-phase theory and spray atomization at engine-relevant conditions, Phys. Fluids 28 (2016) 042108.

[12] R.N. Dahms, J. Manin, L.M. Pickett, J.C. Oefelein, Understanding high-pressure gas-liquid interface phenomena in Diesel engines, Proc. Combust. Inst. 34 (2013) 1667-1675.

[13] R.N. Dahms, J.C. Oefelein, On the transition between two-phase and single-phase interface dynamics in multicomponent fluids at supercritical pressures, Phys. Fluids 25 (2013).

[14] R.N. Dahms, J.C. Oefelein, Liquid jet breakup regimes at supercritical pressures, Combust. Flame 162 (2015) 3648-3657.

[15] R.N. Dahms, J.C. Oefelein, Atomization and dense-fluid breakup regimes in liquid rocket engines, J. Propul. Power 31 (2015) 1221-1231.

[16] C. Crua, J. Manin, L.M. Pickett, On the transcritical mixing of fuels at diesel engine conditions, Fuel 208 (2017) 535-548.

[17] 3M™ Novec™ 649 Engineered Fluid, product literature available at https://www.3m.com/3M/en_US/company-us/all-3m-products/~/3M-Novec-649-Engineered-Fluid/?N=5002385+3290667401&rt=rud

[18] 3M™ Novec™ 1230 Fire Protection Fluid, product literature available at https://www.3m.com/3M/en_US/novec-us/applications/fire-suppression/

[19] Geyer, D. 1D-Raman/Rayleigh experiments in turbulent-opposed jet flows. PhD thesis, Technische Universität Darmstadt, Germany, ISBN 3-18-353306-5, 2005.

[20] Fuest, F. Raman-Spektren diatomarer Moleküle: Eine Optimierung der Spektren Simulation. Diploma thesis, TU Darmstadt, Energie- und Kraftwerkstechnik, 2006.

[21] I.W. Ekoto, R.S. Barlow, Development of a Raman spectroscopy technique to detect alternate transportation fuel hydrocarbon intermediates in complex combustion environments, SAND2012-10389.

[22] G. Magnotti, U. KC, P.L. Varghese, R.S. Barlow, Raman spectra of methane, ethylene, ethane, dimethyl ether, formaldehyde and propane for combustion applications, JQSRT 163 (2015) 80–101.

[23] F. Fuest, R.S. Barlow, D. Geyer, F. Seffrin, A. Dreizler, A hybrid method for evaluation of 1D Raman spectroscopy," Proc. Combust. Inst. 33 (2011) 815–822.